SPECIAL ISSUE ARTICLE

EJN European Journal of Neuroscience   FENS   WILEY

A walk in the park? Characterizing gait-related artifacts in mobile EEG recordings

Nadine Svenja Josée Jacobsen[1] 🄳 | Sarah Blum[1] | Karsten Witt[2] | Stefan Debener[1]

[1]School of Medicine and Health Sciences, Department of Psychology, Neuropsychology Lab, University of Oldenburg, Oldenburg, Germany

[2]School of Medicine and Health Sciences, Department of Neurology and Research Center Neurosensory Science, University of Oldenburg, Oldenburg, Germany

Correspondence
Nadine Jacobsen, University of Oldenburg, School of Medicine and Health Sciences, Department of Psychology, Neuropsychology Lab, Ammerländer Heerstr. 114-118, D-26111 Oldenburg, Germany.
Email: nadine.jacobsen@uni-oldenburg.de

Abstract

Brain activity during natural walking outdoors can be captured using mobile electroencephalography (EEG). However, EEG recorded during gait is confounded with artifacts from various sources, possibly obstructing the interpretation of brain activity patterns. Currently, there is no consensus on how the amount of artifact present in these recordings should be quantified, or is there a systematic description of gait artifact properties. In the current study, we expand several features into a seven-dimensional footprint of gait-related artifacts, combining features of time, time-frequency, spatial, and source domains. EEG of $N = 26$ participants was recorded while standing and walking outdoors. Footprints of gait-related artifacts before and after two different artifact attenuation strategies (after artifact subspace reconstruction (ASR) and after subsequent independent component analysis [ICA]) were systematically different. We also evaluated topographies, morphologies, and signal-to-noise ratios (SNR) of button-press event-related potentials (ERP) before and after artifact handling, to confirm gait-artifact reduction specificity. Morphologies and SNR remained unchanged after artifact attenuation, whereas topographies improved in quality. Our results show that the footprint can provide a detailed assessment of gait-related artifacts and can be used to estimate the sensitivity of different artifact reduction strategies. Moreover, the analysis of button-press ERPs demonstrated its specificity, as processing did not only reduce gait-related artifacts but ERPs of interest remained largely unchanged. We conclude that the proposed footprint is well suited to characterize individual differences in gait-related artifact extent. In the future, it could be used to compare and optimize recording setups and processing pipelines comprehensively.

KEYWORDS

artifact, gait, MoBI, mobile EEG

1 | INTRODUCTION

Little is known about the cortical signatures of gait, possibly because most neuroimaging technologies do not tolerate gross motion well and, therefore, the recording of neural data during motion remains a challenge. Yet, understanding the brain dynamics of gait is important not only to control lower extremity exoskeletons for assisted walking (Venkatakrishnan, Francisco, & Contreras-Vidal, 2014) but also to identify the neural correlates of altered gait patterns. For example, changes in gait characteristics may be a precursor of cognitive decline, as they have been observed as early as 12 years before the onset of a mild cognitive impairment (Buracchio, Dodge, Howieson, Wasserman, & Kaye, 2010). Walking has been linked to increased brain activity in the premotor area, the supplementary motor area (SMA), the pre-SMA and frontal and prefrontal cortex (for a review, see Hamacher, Herold, Wiegel, Hamacher, & Schega, 2015). Changes in gait-related brain activity may provide deeper insights into early signs of neurodegeneration than the measurement of gait characteristics alone.

Recent advances in mobile brain/body imaging (MoBI) techniques allow the study of cortical activity during natural whole-body movements while simultaneously capturing body motion (Gramann, Ferris, Gwin, & Makeig, 2014; Makeig, Gramann, Jung, Sejnowski, & Poizner, 2009). Mobile electroencephalography (EEG) can capture cortical activity with a high temporal resolution during natural walking outdoors (De Vos, Gandras, & Debener, 2014; Debener, Minow, Emkes, Gandras, & de Vos, 2012; Pizzamiglio, Abdalla, Naeem, & Turner, 2018; Pizzamiglio, Naeem, Abdalla, & Turner, 2017; Reiser, Wascher, & Arnau, 2019). This requires combining EEG with motion sensors, like accelerometers and gyroscopes, which capture gait events in natural outdoor environments with high temporal accuracy (Anwary, Yu, & Vassallo, 2018).

During motion, EEG recordings are prone to be contaminated by non-neural activity originating from physiological (e.g., electro-ocular, electromyographic [EMG]) and non-physiological sources (e.g., cable and electrode movement; Castermans, Duvinage, Cheron, & Dutoit, 2014). These artifacts may severely deteriorate signal quality and can be time coupled to the gait cycle, like the cortical activity of interest. Hence, they can hinder an interpretation of the cortical activity and need to be removed from the signal. Simple time-domain averaging procedures for enhancing the signal-to-noise ratio (SNR) do not solve this problem. Recently, temporal, spatial, and frequency properties of gait cycle-related artifacts have been reported (Arad, Bartsch, Kantelhardt, & Plotnik, 2018; Castermans et al., 2014; Gwin, Gramann, Makeig, & Ferris, 2011; Kilicarslan & Contreras Vidal, 2019; Kline, Huang, Snyder, & Ferris, 2015). For instance, head movements can cause artifacts in EEG recordings (O'Regan,

Faul, & Marnane, 2013) that may be coupled to the gait cycle (Hirasaki, Moore, Raphan, & Cohen, 1999). Previous studies already showed that time frequency and power spectra of single EEG channels are similar to the vertical head acceleration during treadmill walking using passive electrodes (Castermans et al., 2014) as well as active electrodes (Kline et al., 2015). Using active electrodes these patterns emerge at higher gait speeds (3 km/hr or greater; Nathan & Contreras-Vidal, 2016). Hence, we expected head acceleration to influence the amount of captured artifactual EEG activity.

It has also been suggested that residual EMG activity might contaminate the activity of different frequency bands (i.e., low-delta and high-gamma) associated with walking (Castermans et al., 2014). EMG as captured by electrodes placed at subjects' necks varied over the gait cycle. Specifically, neck EMG during walking was lateralized, but the pattern was not consistent. On the one hand, EMG of muscles located at the side of the neck displayed broadband power increases around ipsilateral heel strikes (Gwin et al., 2011). On the other hand, broadband power increases following contralateral heel strike in electrodes positioned at the back of the neck were reported (Severens, Nienhuis, Desain, & Duysens, 2012). Interestingly, time courses of neck muscle activity did not show clear modulations over the gait cycle (e.g., Cromwell, Aadland-Monahan, Nelson, Stern-Sylvestre, & Seder, 2001; Richer, Downey, Nordin, Hairston, & Ferris, 2019).

Furthermore, it has been observed that the artifact extent varies over the scalp with greater gait-related artifacts present at central electrodes (Castermans et al., 2014; Kline et al., 2015). These examples indicate that while a coherent characterization of the artifact itself is still lacking, it is necessary to separate physiological from non-physiological EEG signatures successfully.

Studies examining gait-related cortical activity with EEG have applied various artifact reduction strategies. EEG artifact attenuation often includes temporal and spatial filters, channel and epoch rejection, or linear decomposition to facilitate discrimination between signal and artifact. Commonly, independent component analysis (ICA; e.g., Gwin et al., 2011; Makeig, Debener, Onton, & Delorme, 2004; Snyder, Kline, Huang, & Ferris, 2015; Wagner, Makeig, Gola, Neuper, & Müller-Putz, 2016), spectral principal component analysis (Seeber, Scherer, Wagner, Solis-Escalante, & Müller-Putz, 2015), or artifact subspace reconstruction (ASR; Bulea, Kim, Damiano, Stanley, & Park, 2015; Luu, Brantley, Nakagome, Zhu, & Contreras-Vidal, 2017; Nathan & Contreras-Vidal, 2016; Nordin, Hairston, & Ferris, 2019, 2020) and combinations thereof are used. A comprehensive review of previously applied artifact processing strategies is clearly beyond the scope of this study as it was not our goal to identify a single optimal artifact reduction strategy. Moreover, a ground truth about artifact characteristics is

typically not available in EEG data (but see Richer, Downey, Hairston, Ferris, & Nordin, 2020; Richer et al., 2019 for phantom head recordings of emulated treadmill walking including neck muscle activity and artificial neural sources). Instead, we suggest taking a step back and identifying the signal dimensions that could be used to describe the gait artifact comprehensively. Most previous studies used one, or very few features to determine the success of artifact reduction, but different studies used various features, making systematic evaluations across studies difficult. To address this problem, our goal was to develop a standard in the description of the artifact. An established procedure describing gait artifacts should facilitate future work comparing different processing strategies, and it should help to identify hardware most suitable for mobile EEG recording during walking.

Previous authors have used subjective strategies like visual inspection of continuous EEG data (Artoni et al., 2017; Gwin et al., 2011) or gait event-related spectral perturbations (ERSPs; Kline et al., 2015; Nordin, Hairston, & Ferris, 2020), to evaluate the presence of gait artifacts before and after artifact attenuation. They also compared signal-to-noise ratios (SNR) on the sensor or component level (Oliveira, Schlink, Hairston, König, & Ferris, 2016a) or compared event-related potentials (ERP) not locked to the gait cycle (Bruijn, Van Dieën, & Daffertshofer, 2015). The lack of any consensus on the assessment of mobile EEG signal quality limits comparability across studies. To overcome this problem, benchmarking features have been proposed (Oliveira, Schlink, Hairston, König, & Ferris, 2016b). The majority of previously proposed benchmarking features are, however, based on evaluating non-gait-locked ERPs, preventing the application of these features to single-task datasets. However, a non-ERP based feature has been established, the Walking/Sitting ratio (Oliveira et al., 2016b). This feature contrasts EEG power of sitting and walking conditions and is based on the assumption that in the absence of major changes in cortical activity between sitting and walking, similar EEG power would be expected. Yet, broadband EEG power increases during walking compared to sitting have been observed before artifact attenuation (Arad et al., 2018; Oliveira et al., 2016b). In line with this, previous studies uncovered gait cycle event-related oscillatory signatures only after sophisticated artifact processing (Fischer et al., 2018; Seeber et al., 2015; Storzer et al., 2016). Moreover, oscillatory neural activity typically does not change over broad frequency bands in the same direction at the same time, whereas such patterns are generated by non-oscillatory, transient signals, such as artifacts. As gait-related artifacts are not only present in the frequency domain, there is a need to extend features to various other domains and to incorporate the temporal dynamics of a gait cycle. A comprehensive description of the properties of gait-related artifacts would enable evaluation of artifacts across participants, datasets, recording conditions,

and hardware, and hence, contribute to the advancement of artifact attenuation strategies.

In the current study, we expanded several established features into a seven-dimensional footprint of gait-related artifacts. This was done by combining features in the time, time–frequency, spatial, and source domains. To demonstrate the sensitivity to a typical artifact attenuation strategy, we compared the footprint before and after two different stages of artifact processing in an EEG dataset collected during free walking and standing outdoor conditions. We used a reputable attenuation strategy including ASR and ICA (Nordin, Hairston, & Ferris, 2019) to demonstrate the sensitivity of the footprint. To assess the specificity of the artifact reduction, we also evaluated the similarity of the morphologies, topographies and SNRs of button-press ERPs before and after artifact attenuation.

2 | MATERIALS AND METHODS

2.1 | Participants

Data of $N = 26$ young, right-handed, and healthy individuals with normal gait were recorded in this study. Participants were recruited via the online platform of the University of Oldenburg. Before the experiment, they gave written informed consent and received monetary compensation (10€/hr) afterward. The local ethics committee of the University of Oldenburg approved the study (permit number: 2018-079).

2.2 | Materials

EEG data were acquired with 66 Ag/AgCl passive electrodes with a custom 64-channel layout using a subset of the positions in the 10-5 system (Easy Cap GmbH, Herrsching, GER, for channel layout, see Figure S1). For our setup, we combined two 32-channel LiveAmps (Brain Products GmbH). Electrode impedances were kept below 10 kΩ. EEG data were sampled at 500 Hz and online referenced to FCz. The ground electrode was placed at location AFz. The amplifiers were attached to the top of a participant's head using a custom-made sponge containing openings to avoid direct physical pressure on electrodes (see Figure 1a). EEG data were recorded with a lightweight laptop in tablet mode (Ultrabook, Latitude 5289, Dell Inc.) held by the participants. A Bluetooth connection between amplifiers and the laptop was established using the LiveAmpConnector (version 1.16, bit.ly/31P2mrd). The Presentation software (version 20.02, Neurobehavioral Systems, Inc., RRID: SCR_002521) controlled experimental events. Head acceleration was captured with a 3D accelerometer built into the EEG amplifier, and feet acceleration was measured with two 3D accelerometers (eMotion Faros
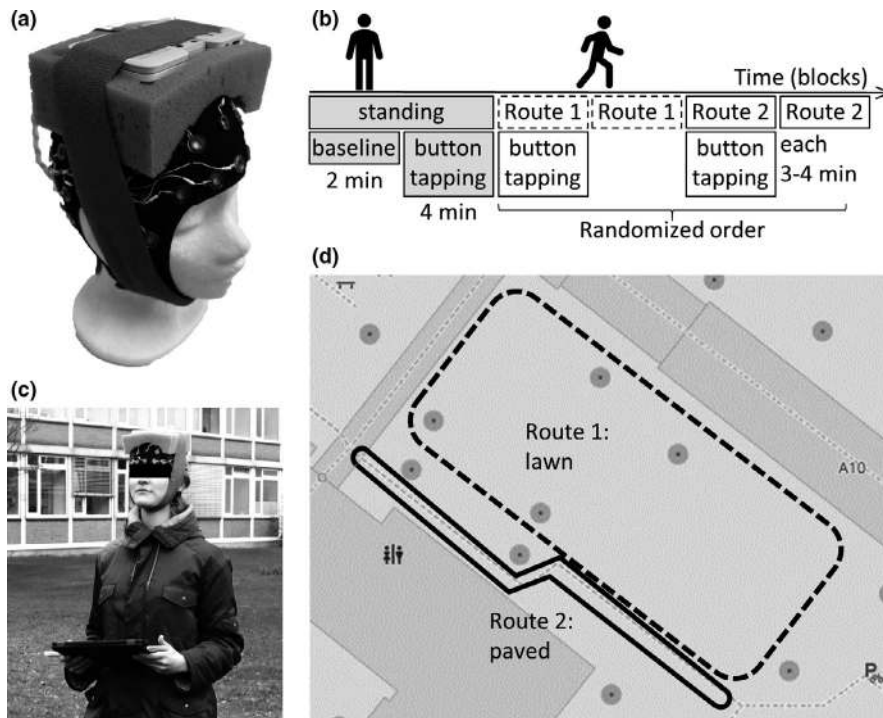
FIGURE 1 (a) 64-channel electrode cap with bundled cables. The wireless amplifier was placed in a customized sponge on top of the subject's head. Recesses in the sponge around the electrodes distributed the weight to non-electrode locations. The sponge–amplifier combo was secured with a self-adhesive bandage wrapped around the subject's head at a comfortable tightness also reducing cap movement. (b) Structure of the outdoors part of the experiment. (c) Subject performing the walking task holding the ultrabook with both hands. (d) The two routes that subjects walked twice, in a randomized order

180°, Mega Electronics Ltd) attached to the top of participants' shoes using self-adhesive bandages. EEG data, head acceleration, and experimental events were synchronized using Lab Streaming Layer and the LabRecorder (version 1.13, bit.ly/2ULAFhb). Data were stored in a single.xdf file and time synchronized to the feet acceleration data offline, using synchronization events inserted into all devices before and after the experiment. After synchronization, each dataset, therefore, consisted of two times 32 EEG channels, one EEG trigger channel, three accelerometer channels from the head, and six accelerometer channels from the feet. Custom scripts were used to extract gait events from the feet acceleration. In pilot recordings, accurate timing of gait events was validated with a motion capture system (Vicon, Oxford, UK). The average temporal error was around 2 ms and deemed acceptable. Data are available at OpenNeuro (https://openneuro.org/datasets/ds003039) and scripts can be found at GitHub (https://doi.org/10.5281/zenodo.4005945).

2.3 | Procedure

The experiment consisted of two parts. Indoors, participants only performed a self-paced gait initiation task but no continuous free walking. This study reports outdoor data only. Outdoors, a standing baseline of 2 min was recorded, and then participants performed a self-paced button-pressing task for 4 min (see Figure 1b,c). During the button-pressing task, individuals were instructed to press buttons displayed on the touchscreen of the laptop in their hands with their left or right thumb. A sound confirmed each successful button

press. Individuals were told to surprise the experimenter about the side and the actual time of each button press and to wait for approx. 1–3 s between button presses. In previous, unpublished studies, we found this instruction to evoke clear readiness potentials. These are slow-cortical potentials preceding self-paced voluntary movements (Kornhuber & Deecke, 1965), which are followed by movement-related cortical potentials (MRCP) occurring around the time of a motor response (Hallett, 1994). Subsequently, participants walked at their preferred speed across campus on two different routes (see Figure 1d), which were marked with pylons. Walking each route took approximately 4 min. Both routes were walked twice by the participants, in a randomized order. On each route, participants performed the button-pressing task, as described above, once. Participants were instructed to fixate their gaze to a point at eye level and to avoid unnecessary head movements and jaw clenching during EEG recording.

2.4 | EEG analysis

EEG data were processed using EEGLAB (version 14.1.2, Delorme & Makeig, 2004, RRID:SCR_007292), Brainstorm (version Jan 2020, Tadel, Baillet, Mosher, Pantazis, & Leahy, 2011, RRID:SCR_001761) and custom code in MATLAB (version R2018b, MathWorks Inc., RRID:SCR_001622). The EEG preprocessing is outlined in Figure 2. The scripts used for the calculation of the footprint are accessible on GitHub (https://doi.org/10.5281/zenodo.4005945).
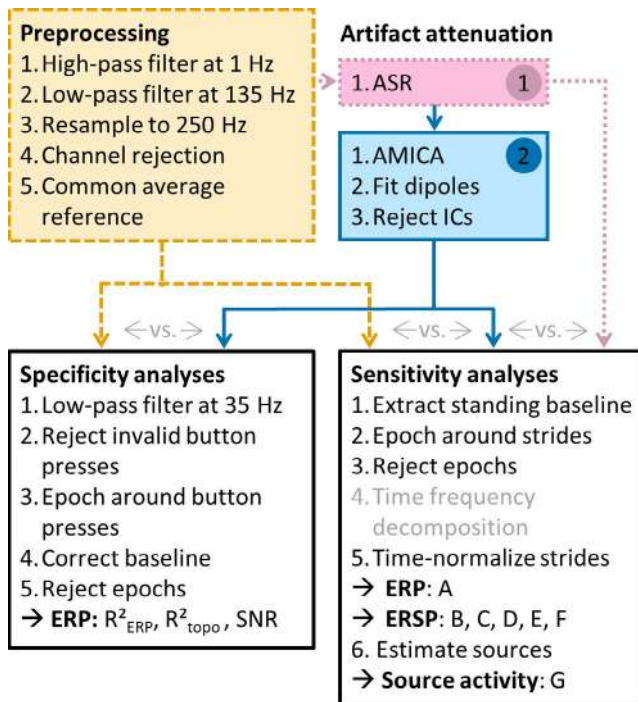
Preprocessing
1. High-pass filter at 1 Hz
2. Low-pass filter at 135 Hz
3. Resample to 250 Hz
4. Channel rejection
5. Common average reference

Artifact attenuation
1. ASR ①

1. AMICA ②
2. Fit dipoles
3. Reject ICs

⟵vs.⟶

Specificity analyses
1. Low-pass filter at 35 Hz
2. Reject invalid button presses
3. Epoch around button presses
4. Correct baseline
5. Reject epochs
→ ERP: R^2_{ERP}, R^2_{topo}, SNR

⟵vs.⟶   ⟵vs.⟶

Sensitivity analyses
1. Extract standing baseline
2. Epoch around strides
3. Reject epochs
4. Time frequency decomposition
5. Time-normalize strides
→ ERP: A
→ ERSP: B, C, D, E, F
6. Estimate sources
→ Source activity: G

FIGURE 2 Overview of the electroencephalography (EEG) analysis pipeline. First, raw EEG data were preprocessed (dashed line) and then artifact attenuated using artifact subspace reconstruction (stage 1, dotted line) and subsequently independent component analysis (stage 2, solid line). All datasets underwent sensitivity analyses, resulting in footprint features of the time, time–frequency, spatial, and source domain. Footprints of preprocessed data and data at stage 2, as well as footprints of data at stage 1 and 2, were compared. Moreover, specificity analyses allowed to compare morphologies and topographies before and after artifact processing

2.4.1 | Preprocessing

First, EEG data were high-pass filtered at 1 Hz (order 826) and low-pass filtered at 135 Hz (order 56) with the zero-phase, finite impulse response (FIR) filters (*eegfiltnew*) and then downsampled to 250 Hz. Bad channels were identified using the *clean_rawdata* toolbox (flatline channels for 5 s, channel correlation below 0.8, and line noise above 4, other parameters disabled; version 2.1). Note that the correction function of the ASR toolbox was not applied here. Subsequently, the data were re-referenced to the common average.

2.4.2 | Artifact attenuation

We chose to attenuate gait-related and other artifacts, like blinks, with previously used techniques, specifically a combination of ASR (Mullen et al., 2015) and ICA. In contrast to other studies (Artoni et al., 2017; Bulea et al., 2015; Gwin, Gramann, Makeig, & Ferris, 2010; Gwin et al., 2011; Lau,

Gwin, & Ferris, 2014; Sipp, Gwin, Makeig, & Ferris, 2013; Wagner et al., 2012, 2016; Wagner, Martínez-Cancino, & Makeig, 2019; Wagner, Solis-Escalante, Scherer, Neuper, & Müller-Putz, 2014), we refrained from clustering ICs across subjects, as our artifact attenuation impact was evaluated on a single-subject level. Furthermore, artifact extent was evaluated at the sensor level to allow comparisons of data before and after various preprocessing methods not limited to ICA.

Following preprocessing, the ASR algorithm was applied. ASR attempts to correct artifacts in continuous, non-stationary EEG data by performing a principal component analysis on sliding windows and finding deviations to reference data obtained in an initial calibration session. Potentially artifactual data segments are subsequently corrected using information gathered in the calibration phase and clean portions of the current segment. ASR was calibrated on 1-min standing baseline recordings and a cutoff of standard deviation (SD) of 7 was chosen, following Nordin et al. (2019). Data processed up to this stage are referred to as artifact attenuated 1.

Subsequently, the walking conditions and the remaining standing baseline were concatenated. For ICA attenuation, consecutive 1-s epochs were extracted and epochs with a joint probability exceeding a threshold of $SD = 3$ were rejected using EEGLAB's function *jointprob*. On the remaining data, an adaptive mixture independent component analysis (AMICA; Palmer, Kreutz-Delgado, & Makeig, 2011) was performed and the obtained weights were back-projected to the continuous data. AMICA decomposition was chosen in line with several other studies (e.g., Arad et al., 2018; Artoni et al., 2017; Bradford, Lukos, & Ferris, 2016; Bulea et al., 2015; Gwin & Ferris, 2012; Gwin et al., 2010, 2011; Lau et al., 2014; Nordin et al., 2019, 2020; Sipp et al., 2013; Wagner et al., 2012, 2016), as it achieved greater mutual information reduction and more near-dipolar ICs (Delorme, Palmer, Onton, Oostenveld, & Makeig, 2012). AMICA was also found to attenuate EMG artifacts during treadmill walking better than InfoMax (Bell & Sejnowski, 1995; Leutheuser et al., 2013). Following ICA, previously rejected channels were interpolated and dipoles were fitted using DIPFIT (version 3.2, Oostenveld, Delorme, & Makeig, 2003). A three-layer boundary element model (BEM) and the default anatomy were chosen. Only ICs with dipoles located inside the head and a residual variance lower than 15% were kept. ICs were also automatically classified using IClabel (Pion-Tonachini, Kreutz-Delgado, & Makeig, 2019). Components exceeding a 90% probability of being eye, muscle, heart, line noise, and channel noise were rejected. Remaining ICs were back-projected to the sensor space. Data cleaned with ASR and, subsequently, ICA were called artifact attenuated 2. Without further specification, data referred to as 'artifact attenuated' are data cleaned at stage 2 (including ASR and ICA).

TABLE 1 Description of footprint features and their mean and standard deviation before and after artifact handling

Feature	Motivation	Quantification	Before ($M \pm SD$)	Stage1 ($M \pm SD$)	Stage 2 ($M \pm SD$)
A. EEG activity explained by head acceleration	Head movements cause artifacts and are coupled to the gait cycle.	Squared correlation of the root mean square of head acceleration and the global field potential.	0.52 ± 0.23	0.14 ± 0.14	0.10 ± 0.08
B. Frequency correlations	A consistently high coupling over a broad frequency range may indicate EEG data of non-neural origin.	The average correlation of all frequency time-courses squared.	0.95 ± 0.03	0.93 ± 0.03	0.93 ± 0.04
C. Lateral to all channel power Ratio	A large fraction of EEG activity recorded during walking at lateral electrodes may be artifactual.	The ratio of the total power of half the more lateral electrodes to the total power of all electrodes.	0.49 ± 0.29	0.58 ± 0.03	0.12 ± 0.23
D. Neck channel power ratio	Electrodes located over neck muscles show strong power increases following contralateral heel strike.	The ratio of power during double supports of neck channels contralateral to the previous heel strike to power at the ipsilateral ones subtracted from 1.	0.65 ± 0.07	0.15 ± 0.16	0.56 ± 0.03
E. The double support power ratio	A strong, broadband power increase can be observed during double support in the grand mean ERSP.	The ratio of total power during the double support phase to the total power of the gait cycle.	0.42 ± 0.07	0.37 ± 0.03	0.37 ± 0.03
F. Standing/ walking power ratio	EEG power of standing and walking might be similar.	The ratio of standing EEG power to walking EEG power subtracted from 1.	0.20 ± 0.25	-0.05 ± 0.17	-0.06 ± 0.22
G. M1 source activity	Source estimation identifies relatively more activity in cortical areas associated with leg motor control compared to the remaining cortex.	The ratio of normalized source activity at leg motor ROI to normalized source activity of the remaining cortex.	0.75 ± 0.30	0.78 ± 0.24	0.97 ± 0.21

Note: Observed feature values at different stages of artifact attenuation. After preprocessing (before), after ASR (stage 1) and after ASR and ICA (stage 2).

Abbreviations: ASR, artifact subspace reconstruction; EEG, electroencephalography; ICA, independent component analysis; *M*, mean, *SD*, standard deviation.

2.4.3 | Sensitivity analysis: Gait-artifact–related footprint

EEG activity time locked to gait events were used to calculate a set of seven features of gait-related artifacts. EEG data were processed as follows to enable the calculation of these footprint features. A summary of all features can be found in Table 1. Gait epochs were generated using the right heel strikes (RHS) as time-locking events. Epochs in which the consecutive right heel strikes were further than 1.5 s apart, epochs in which the order of gait events was abnormal (not in the order: RHS, left toe-off (LTO), left heel strike (LHS), right toe-off (RTO), RHS), and epochs with abnormal activity (joint probability of $SD > 3$) were rejected. The remaining data were submitted to a time–frequency transform using linearly spaced, three-cycle Morlet wavelets from 4 to 60 Hz in 1 Hz steps (*newtimef*). All epochs were time warped to equal length, using the latencies of all gait events in one gait cycle. ERSP power was baseline corrected by dividing by the mean power of the standing baseline. The

resulting, baseline-corrected ERSPs were used to calculate footprint features B, D, E, and F. EEG sources of the individual, time-normalized gait ERP were estimated using Brainstorm. The default anatomy provided by the software and a three-layer BEM (as implemented in openMEEG, Gramfort, Papadopoulo, Olivi, & Clerc, 2010) were chosen. Noise covariance was calculated from standing baseline data and source signals were estimated using dynamical statistical parametric mapping (dSPM) (Dale et al., 2000) with a minimum norm estimator (MNE) and a constrained dipole orientation. Source activity was smoothed with a 3 mm full-width-half-maximum (FWHM) kernel. Obtained source activity was used to calculate feature G.

2.4.3.1 | A. EEG activity explained by head acceleration

The 3D head accelerations were 1 Hz high-pass filtered in the same manner as the EEG data (zero-phase FIR filters, order 826) to attenuate effects of gravity and also epoched around the RHS. Epochs were subsequently time normalized

and averaged. The extent of head acceleration was then quantified as the root mean square (RMS) of this time series. The EEG RMS was calculated as the spatial standard deviation, also known as global field potential (GFP; Skrandies, 1990) of the time-normalized gait cycle ERP of each dataset. Both calculations resulted in a single time series. As peaks of the EEG GFP occurred slightly later than the peaks of the acceleration RMS, we cross-correlated the RMS of the head acceleration with the zero-mean GFP using *xcorr*, tolerating a maximum lag of ±5 samples. Cross-correlations were normalized so that the zero-lag autocorrelation was 1. We then squared the highest obtained correlation to obtain a measure of explained variance (R^2). We assumed that the GFP of the gait ERP was linked to the gait cycle and the RMS of head acceleration before artifact attenuation. We expected the coupling to be weakened by artifact attenuation 1 and to a greater extent by artifact attenuation 2. This pattern should be reflected by decreased R^2 values.

2.4.3.2 | B. Explained variance across frequencies

As a consistently high coupling over a broad frequency range may well serve to indicate EEG data of non-neural origin, we correlated the time courses of all frequency power profiles (4–60 Hz, 1 Hz steps) with each other. We then obtained the mean correlation across frequencies. To do so, the correlation matrix was Fishers Z-transformed to approximate a normal distribution (Fisher, 1915). We subsequently calculated the mean correlation of the upper triangle, thus, excluding autocorrelations. The resulting mean correlation was inverse transformed and squared to get the coefficient of determination (R^2). R^2 here indicates the amount of variance in the time course of one frequency explained by the other frequencies. We assumed a decreased value after artifact processing if the broadband activity was reduced and frequency band-specific changes emerged. A smaller decrease was expected for artifact attenuation 1 than 2.

2.4.3.3 | C. Lateral to all channel power ratio

We summed each channel's ERSP across time and frequency. We then aggregated the power of 50% of the more lateral electrodes (Fpz, Fp1, Fp2, AF7, AF8, F7, F8, F9, F10, FT7, FT8, FT9, FT10, T7, T8, TP7, TP8, TP9, TP10, P7, P8, P9, P10, PO7, PO8, PO9, PO10, Oz, O1, O2, I1, and I2) and calculated their share of the total power of all electrodes. This ratio should decrease after artifact attenuation because much of the activity on these channels may be generated by non-cortical activity, which should be reduced after artifact attenuation. A weaker reduction was expected for artifact attenuation 1 than 2.

2.4.3.4 | D. Neck channel power ratio

We accumulated the power of subjects' ERSPs across all frequencies and channels. We then extracted samples during double support and summed power of channels located at the neck contra- and ipsilateral to the previous heel strike (left neck: PO7, PO9, O1, I1; right neck: PO8, PO10, O2, I2). Subsequently, we subtracted the ratio of the ipsilateral to the contralateral neck power from 1. This ratio is zero if broadband power at ipsi- and contralateral neck channels are equal. It is greater than zero if the power of contralateral channels is greater than the power of ipsilateral channels and smaller than zero if the power of contralateral channels is smaller than the power of ipsilateral channels. If the asymmetry of EMG artifacts decreased after artifact attenuation, so should the value of this ratio. A smaller decrease was expected for artifact attenuation 1 than 2.

2.4.3.5 | E. Double support power ratio

We added the power of all frequencies and channels and extracted the summed power during the double support phase as well as the summed power of the whole gait cycle. Subsequently, the ratio of the power during the double support phase to the total power over the gait cycle was calculated. We expected both artifact attenuation pipelines to reduce this ratio, but pipeline 1 to a smaller degree than pipeline 2.

2.4.3.6 | F. Standing/walking power ratio

We adapted the established walking/sitting power ratio (Oliveira et al., 2016b) to a standing/walking power ratio. We calculated the ratio of standing EEG power to walking EEG power and subtracted the resulting value from 1 to attain a similar scale to the remaining proposed features. The resulting value is zero when the power during standing is the same as during walking. Positive values result from power during walking being higher than during standing, which can be expected for non-artifact attenuated data. After artifact attenuation, event-related alpha and beta power decreases (i.e., desynchronization) during walking compared to standing have been reported (Seeber, Scherer, Wagner, Solis-Escalante, & Müller-Putz, 2014), potentially resulting in decreased broadband power during walking compared to standing and again, a smaller value of this feature. We reasoned that artifact attenuation 2 might decrease this feature stronger than artifact attenuation 1.

2.4.3.7 | G. ROI source activity

We suggest that source estimation identifies relatively more prominent activity in cortical areas associated with walking (e.g., the premotor area and the SMA) compared to the remaining cortex. We used a gait initiation task to identify a leg motor control region of interest (ROI) in each hemisphere in the same sample (for details see supplemental material). This ROI was located over the central part of the precentral gyrus and the posterior part of the superior frontal gyrus, reaching into the interhemispheric cleft. Source activity was extracted from this ROI as well as from the remaining cortex

and accumulated over the whole gait cycle. Both values were then normalized by the number of included vertices (ROI: 350 vertices, remaining cortex: 14,652 vertices). The per-vertex activity of the remaining cortex was then divided by the activity per vertex of the ROI. A similar average activity in both areas results in a value of 1. Whereas if the activity at the ROI is higher than at the remaining cortex, the value decreases, which indicates greater estimated activity at the chosen ROI than the remaining cortex. Hence, if artifact attenuation largely reduced activity outside of the ROI than within this value would decrease. This decrease might be stronger following artifact attenuation stage 2 than stage 1.

2.4.4 | Specificity analysis

The presence of a non-gait–related signal can be evaluated before and after artifact processing to assess the specificity of any artifact attenuation pipeline. It was not our goal to identify the most powerful artifact reduction strategy, as this may depend on the specific research questions. We, therefore, performed the specificity analysis following artifact attenuation stage 2, exploring whether the neural activity of interest remained unchanged by the correction of unwanted signals. A specific artifact handling would retain the signal of interest while reducing the noise, thus, improving the SNR. Here, the MRCP of self-paced thumb button presses during walking, and the auditory evoked potential (AEP) N1 following the feedback tone elicited by the button press, were used. The change in signal following artifact attenuation was evaluated by comparing morphologies, topographies, and SNRs of all three ERPs (MRCP left thumb, MRCP right thumb, and AEP N1). Accordingly, the following pipeline was performed twice, once with only preprocessed EEG data and once with preprocessed and artifact attenuated EEG data following ASR and ICA (see Figure 2). First, EEG data were low-pass filtered at 45 Hz (zero-phase FIR filter, order: 84). Button presses that were less than 800 ms apart from each other were removed, to not interfere with the AEP response, and allow for an appropriate baseline for the next button press epoch. Epochs were extracted from −500 to 500 ms around each button press and baseline corrected from −500 to −300 ms. Epochs with artifactual activity, identified by values exceeding a joint probability of $SD = 3$, were rejected. From 342 (range: 149 to 563) button presses with both thumbs, on average 120 (range: 25 to 225) left thumb and 124 (range: 20 to 195) right thumb button presses remained before artifact attenuation. After artifact handling, on average 109 (range: 22 to 208) left thumb and 110 (range: 18 to 171) right thumb button presses remained in the data per subject. Sources of the artifact-attenuated button-press ERP averaged across subjects were calculated with Brainstorm for illustrative purposes. We used the default anatomy provided by the

software, a three-layer BEM, and a noise covariance computed from the ERP baseline (−500 to −300 ms). Sources were estimated using dSPM with MNE and a fixed orientation. Source activity was smoothed with a 3 mm FWHM kernel.

2.5 | Statistical analysis

Statistical analyses were performed in R (version 3.4.2, R Core Team, 2017). Shapiro–Wilk tests assessed normality (of differences), before performing Student's t tests. Where indicated, a non-parametric alternative, i.e., the Wilcoxon signed-rank test, was used. Alpha levels were kept at 0.05. p-values were Bonferroni–Holm corrected for multiple comparisons. Effect sizes were provided as Cohen's d (t test) or R (Wilcoxon).

2.5.1 | Sensitivity analysis

Euclidean distance values between the footprint feature vector before and after artifact attenuation stage 2 and between artifact attenuation stage 1 and 2 were calculated. Their deviation from zero was tested with one-sided, one-sample Student's t tests. Single features were statistically compared before and after artifact attenuation (stage 2) with two-sided, dependent samples Student's t tests or, if indicated, with Wilcoxon signed-rank tests for dependent samples. Pearson's correlation coefficients between the features were calculated before and after artifact attenuation to evaluate whether they provide redundant information.

2.5.2 | Specificity analyses

Both the MRCP and the N1 of the button presses were evaluated using three different measures. First, topographies of all three ERPs were compared before and after artifact attenuation. Topographies were created by averaging data points centered on the peak response (MRCP: −110 to −10 ms, N1: 150 to 170 ms). Topographies before and after artifact reduction were correlated and the Fisher Z-transformed values submitted to a two-sided, one-sample Student's t test. Secondly, time courses of all three ERPs at the respective ROI (MRCP left: C2, CP2, C4, CP4; MRCP right: C1, CP1, C3, CP3; N1: Fz, FC1, FC2, Cz) were correlated before and after artifact attenuation. This was done from −100 to 300 ms including the MRCP and the AEP. Correlations were Fisher z-transformed. A two-sided, one-sample Student's t test was used to test whether the obtained values differed significantly from zero, which would indicate that the ERP morphology before and after artifact processing was significantly correlated. Thirdly, the ERP SNR in decibel (dB) was calculated as follows: $SNR = 10 * \log_{10}(\frac{signal}{noise})$. Signal

strength was estimated as the mean voltage of the corresponding time window (MRCP: −110 to −10 ms, N1: 150 to 170 ms) and ROI. The noise was estimated on the ERP averaged over the corresponding ROI as the standard deviation of the baseline from −500 to −300 ms before a button press. SNRs before and after artifact processing were compared using a two-sided, dependent-samples Student's t test.

3 | RESULTS

3.1 | Participants

In total, $N = 10$ subjects were excluded from the analysis for the following reasons: problems with the recording software ($n = 5$), failure to send the synchronization triggers appropriately ($n = 1$), not meeting the inclusion criteria ($n = 1$), and failure to comply with task instructions ($n = 3$). Task instructions were not followed by performing button presses too fast (less than 20 trials ≥ 0.8 s apart, $n = 2$) or initiating gait not at least 20 times with each leg, $n = 1$). After exclusion, $n = 16$ participants (age 24 ± 4 years, 14 females) were available for the statistical analyses.

3.2 | Preprocessing

Per participant, on average 1.5 (range: 0 to 4) channels were removed and 28 (range: 18 to 32) independent components remained after artifact attenuation stage 2. After preprocessing, on average 712 gait cycles (range: 501 to 787) remained per subject. After ASR 667 gait cycles (range: 494 to 790) and after subsequent ICA 696 gait cycles (range: 509 to 803) remained on average per participant.

3.3 | Sensitivity analysis: gait-artifact–related footprint

We compared the footprint as a multidimensional evaluation of gait-related artifacts before and after two artifact attenuation stages. A composite score of the footprint, namely, the Euclidean distance between all feature vectors, confirmed significant differences before and after artifact processing using ASR and ICA ($M = 0.82$, $SD = 0.22$, $t_{15} = 14.58$, $p < .001$, $d = 3.65$). Furthermore, footprints following only ASR and footprints following ASR and ICA were different ($M = 0.32$, $SD = 0.14$, $t_{15} = 9.18$, $p < .001$, $d = 2.29$, see Figure 3). Means and standard deviations before and after artifact reduction following ASR and ICA can be found in Table 1 and are illustrated in Figure 3a. The results of each feature are described in the following.

Before artifact attenuation feature B was correlated with feature E ($r = .74$, $p = .022$, $R = .55$). After artifact attenuation using ASR and ICA, none of the features remained significantly correlated (Figure 4).

3.3.1 | A. EEG activity explained by head acceleration

As expected, the RMS of the head acceleration and the EEG GFP were systematically coupled to the gait cycle. RMS of head acceleration showed a distinct pattern over
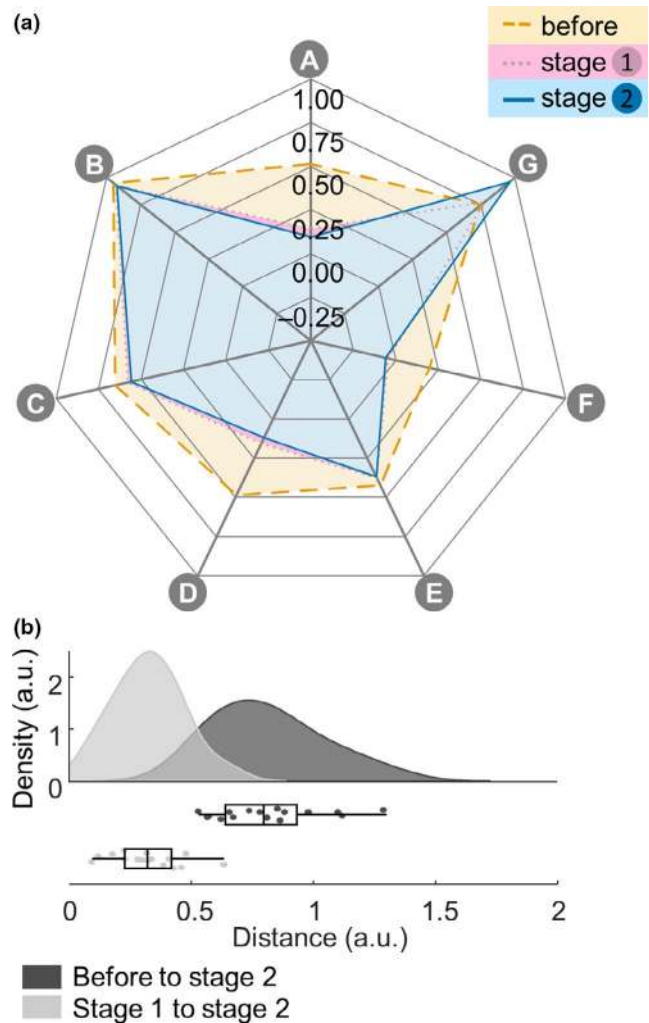

FIGURE 3 (a) All features of the proposed footprint at different processing stages: before artifact attenuation (dashed line), after artifact subspace reconstruction (ASR; stage 1, dotted line), and after ASR and independent component analysis (stage 2, solid line). Smaller values indicate reduced gait-related artifacts. (b) Euclidean distances of footprint feature vectors of preprocessed data to data at stage 2 (dark grey) and of data at stage 1 to stage 2 (light grey). Dots represent single subjects
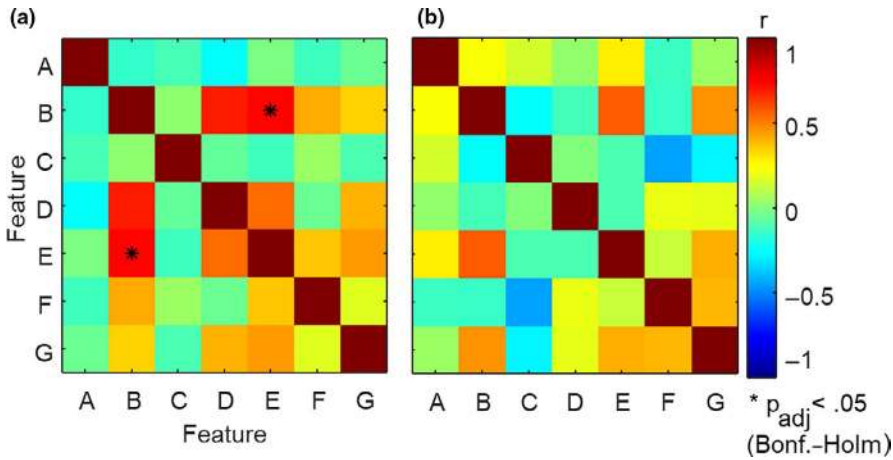
FIGURE 4 Pearson correlation matrices of the footprint features before (a) and after artifact subspace reconstruction and independent component analysis artifact attenuation (stage 2, b). Significant correlations ($p_{adjusted} < .05$) marked with asterisks

the averaged, time-normalized gait cycle, peaking during double supports independent of the side of the heel strike (see Figure 5). Another smaller peak occurred during the single support phases. The pattern of the GFP of the time-normalized, uncorrected gait ERP looked similar. After artifact processing, the GFP was reduced in amplitude and did not show a systematic variation with the gait cycle anymore as reflected by the significant reduction in explained variance ($M_{diff} = -0.42$, $SD_{diff} = 0.22$, $T_{15} = -7.64$, $p < .001$, $d = -2.29$). Using ICA after ASR did not change obtained values of feature A ($M_{diff} = -0.05$, $SD_{diff} = 0.12$, $T_{15} = -1.54$, $p = .143$).

3.3.2 | B. Explained variance across frequencies

Time courses of frequencies from 4 to 60 Hz behaved in a similar manner across the averaged, time-normalized gait cycle (see Figure 6). Compared to a standing baseline, their power peaked during double supports before, as well as after artifact attenuation. After artifact handling, amplitudes of all frequencies were reduced. Yet, the amount of variance in any frequency that was explained by the variance in other frequencies did not decrease in the artifact-corrected data ($M_{diff} = -0.02$, $SD_{diff} = 0.03$, $T_{15} = -0.88$, $p = .393$). Correspondingly, using ICA after ASR did not change the obtained values of feature B significantly ($M_{diff} = 0.00$, $SD_{diff} = 0.02$, $T_{15} = -3.22$, $p = .054$).

3.3.3 | C. Lateral to all channel power ratio

Lateral channels captured median (Mdn) = 0.64 of the total power before artifact attenuation, as illustrated in Figure 7. This was particularly evident at channels located near the subjects' neck. After artifact reduction, power was generally reduced, and only $Mdn = 0.57$ of power originated from lateral channels.
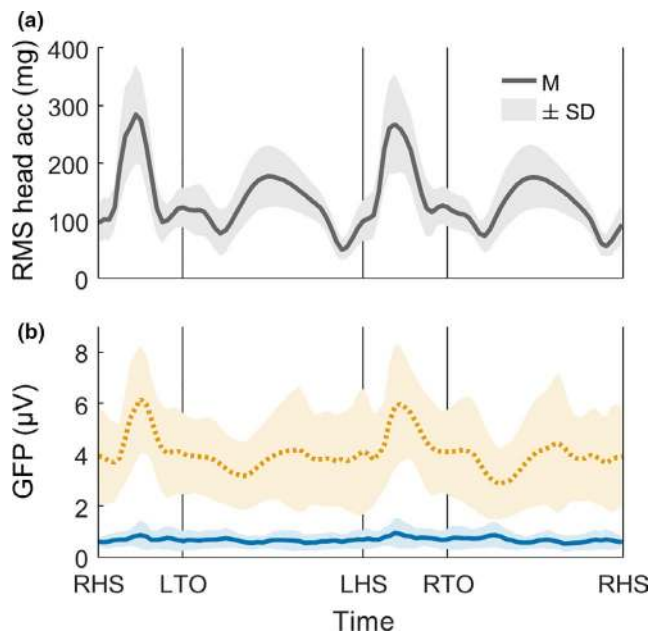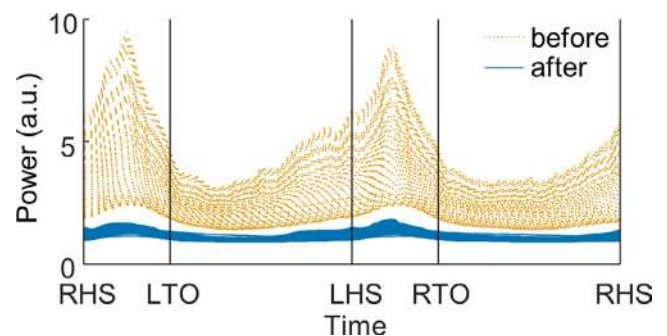

FIGURE 5 Grand mean RMS of head acceleration (a) as well as GFP (b) before (dashed line) and after artifact attenuation (stage 2, solid line) over the time-normalized gait cycle. Shaded areas indicate plus–minus 1 standard deviation across subjects. Gait events are indicated by vertical lines (right heel strike (RHS), left toe-off (LTO), left heel strike (LHS), and right toe-off (RTO))

FIGURE 6 Grand mean time courses of all frequency scales before (dashed line) and after (stage 2, solid line) artifact reduction. Gait events are indicated by vertical lines (right heel strike (RHS), left toe-off (LTO), left heel strike (LHS), and right toe-off (RTO))

This was a significant decrease ($T = 136$, $p < .001$, $R = −1.04$). Nonetheless, an inspection of isopotential lines still hinted at a residual activity at lateral regions, especially near the neck. Performing ICA after ASR further reduced values of feature C ($M_{diff} = −0.02$, $SD_{diff} = 0.02$, $T_{15} = −4.34$, $p = .013$, $d = −0.5$).

3.3.4 | D. Neck channel power ratio

In line with Severens et al. (2012), electrodes located over neck muscles showed strong power increases following contralateral heel strike compared to a standing baseline (see Figure 6a). As this may primarily reflect EMG activity, this feature should be reduced by artifact attenuation. Before artifact reduction the power ratio was positive ($Mdn = 0.57$), indicating that during the double support phases electrodes placed on the side of the neck contralateral to the previous heel strike captured more power than electrodes placed ipsilaterally. After artifact attenuation, this value dropped
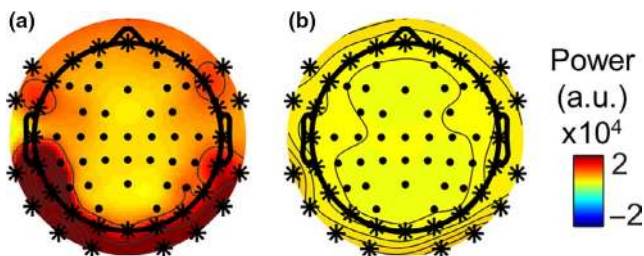

FIGURE 7 Power change to standing baseline before (a) and after (stage 2, b) artifact reduction. Electrodes defined as lateral are marked by an asterisk

significantly ($Mdn = 0.16$, $T = 129$, $p = .010$, $R = −.86$) but remained positive (see Figure 8). Obtained values remained when ICA was performed after ASR ($T = 95$, $p = 1$).

3.3.5 | E. Double support power ratio

Compared to a standing baseline, a strong, broadband power increase, in particular in the higher frequency range, can be observed during double support in the grand mean ERSP, probably largely reflecting artifacts (see Figure 9a). Compared to a standing baseline, the largest power increase during the averaged gait cycle was observed during double support phases. This increase was most pronounced at higher frequencies, echoed by the double support power ratio of $M = 0.42$ ($SD = 0.07$), although double support covered only 32% of the time-normalized gait cycle. After artifact attenuation, power was attenuated across all frequencies and time points (see Figure 9b), as was the power ratio, which decreased to $M_{diff} = −0.06$, $SD_{diff} = 0.04$, $T_{15} = −5.74$, $p < .001$, $d = −0.37$. Obtained values of feature e further decreased when using ICA after ASR ($M_{diff} = −0.01$, $SD_{diff} = 0.021$ $T_{15} = −5.41$, $p < .001$, $d = −0.23$).

3.3.6 | F. Standing/walking power ratio

EEG recorded during walking also showed greater broadband power than EEG recorded during standing before artifact attenuation, as shown in Figures 7 and 9. Before artifact handling, the standing/walking power ratio was greater than zero ($M = 0.20$, $SD = 0.25$, see Figure 10), confirming that, on average, power during walking was higher than power during standing. On
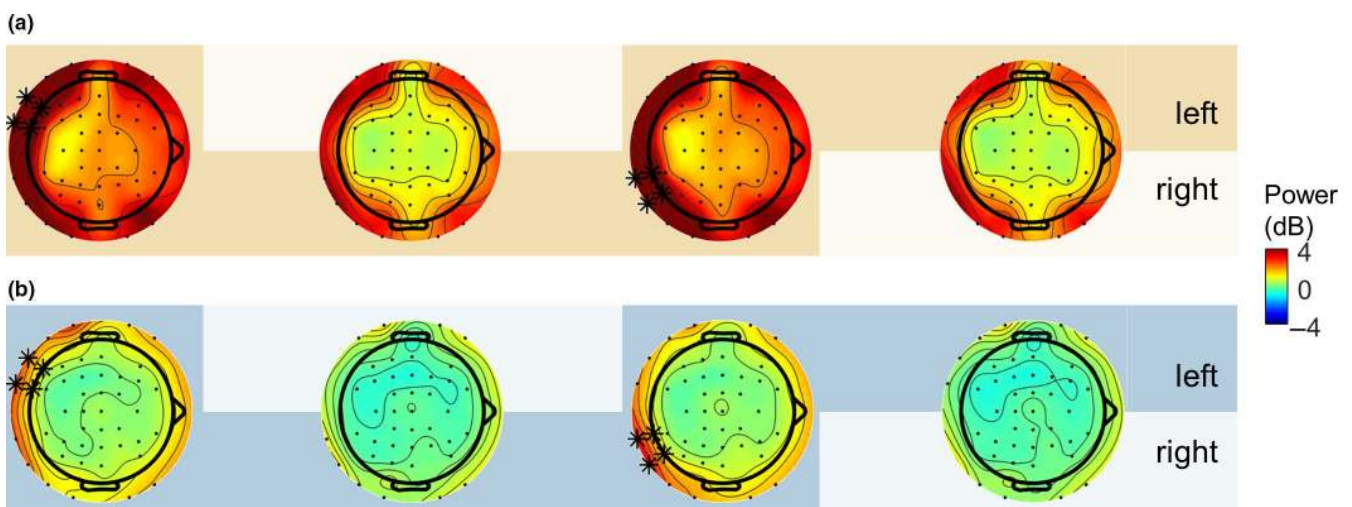

FIGURE 8 Grand mean topographies of mean power change (dB) to a standing baseline from 4 to 60 Hz before (a) and after (stage 2, b) artifact attenuation. The neck channel ratio was calculated during double support. Marked by asterisks are the channels contralateral to heel strike, which were compared to the power of the ipsilateral neck channels. Shaded areas specify durations during which the respective foot was on the ground. Gait events are indicated right heel strike (RHS), left toe-off (LTO), left heel strike (LHS), and right toe-off (RTO)
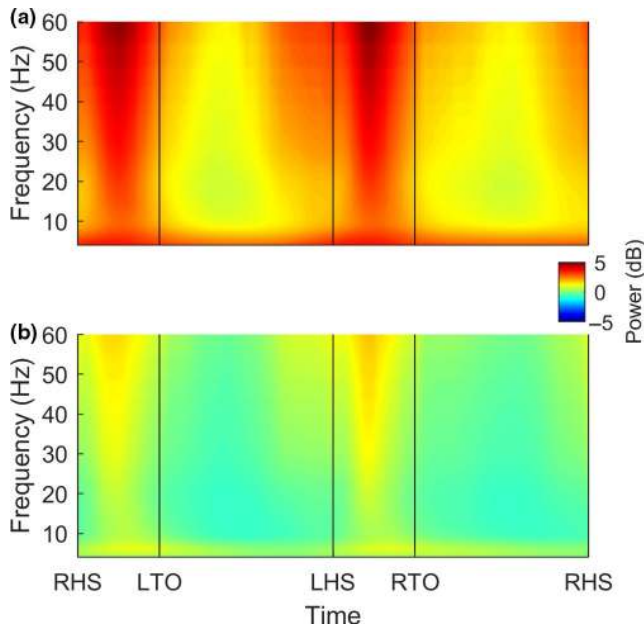
FIGURE 9 Grand mean ERSPs before (a) and after (stage 2, b) artifact attenuation. Power change (dB) relative to a standing baseline. Gait events are indicated by vertical lines (right heel strike (RHS), left toe-off (LTO), left heel strike (LHS), and right toe-off (RTO))

a single subject level, only 1 of 16 participants had less EEG power during walking than standing. After artifact attenuation, the power ratio value dropped ($M_{diff} = -0.26$, $SD_{diff} = 0.20$, $T_{15} = -5.28$, $p < .001$, $d = -1.11$), demonstrating that EEG power was very similar between standing and walking now, as could be expected. Performing ICA after ASR did not further decrease the values of feature F ($M_{diff} = -0.02$, $SD_{diff} = 0.11$, $T_{15} = -0.56$, $p = 1$).

3.3.7 | G. ROI source activity

Source activity in a ROI around M1 leg representation areas was estimated before and after two stages of artifact
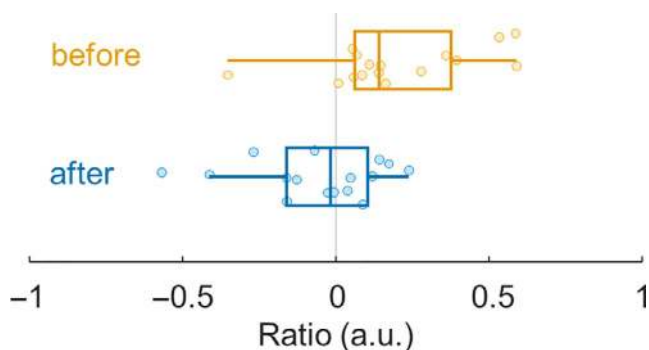

FIGURE 10 Standing/walking ratio before (up) and after (down) artifact attenuation. Dots represent single subject values

attenuation. Before artifact attenuation, the estimated source activity of the dorsal cortex peaked around the interhemispheric cleft, starting around the central sulcus and spanning over the central part of the parietal cortex (see Figure 11). The estimated source activity at the ROI, edged in black, was higher than at the surrounding cortex, resulting in a value of $M = 0.75$. After artifact attenuation, the amplitude of the estimated source activity decreased and the above-mentioned patterns diminished. Yet, the value of the corresponding feature remained the same after artifact attenuation using ASR and ICA ($M_{diff} = 0.21$, $SD_{diff} = 0.34$, $T_{15} = 2.51$, $p = .192$). Conducting ICA after ASR also did not influence this feature ($M_{diff} = 0.18$, $SD_{diff} = 0. 24$, $T_{15} = 3.10$, $p = .084$). Implying that the average activity per-vertex at the ROI was unchanged compared to the values of the remaining cortex after any stage of artifact attenuation than before. Descriptively, this feature increased with subsequent artifact attenuation stages.

3.4 | Specificity analyses

We evaluated button-press ERPs before and after artifact reduction to assess whether a signal of interest remained after artifact attenuation. We compared morphologies, peak topographies, and SNRs of the MRCPs preceding self-paced button presses as well as the AEP N1 on tones given as feedback to the button presses.

Time courses from -100 to 300 ms of the ERPs at the respective ROI before and after artifact attenuation showed significant correlations for both left and right thumb button presses (see Table 2). Averaged topographies from -110 to 10 ms before the button press exhibited contralateral negativity over central electrodes before and after artifact attenuation (see Figure 12b). Before artifact attenuation, topographies additionally displayed a strong positive deflection at frontopolar electrodes. This activity could be reminiscent of eyeblink artifacts. ERP amplitudes were higher before artifact
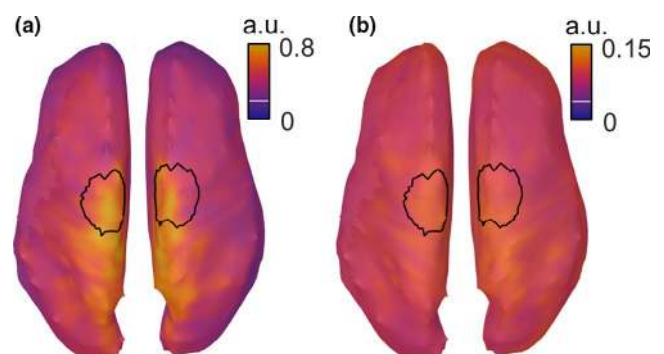

FIGURE 11 Grand mean source estimation of the gait ERP before (a) and after (b) artifact attenuation displayed on the default cortex used by Brainstorm. Borders of the region of interest are contoured

TABLE 2 Fisher Z transformed correlations of the ERP before and after artifact attenuation at the respective ROI

ERP	M	SD	T	df	p_{adj}	d
MRCP left	1.05	0.45	9.39	15	<.001	2.35
MRCP right	1.18	0.39	12.31	15	<.001	3.08
N1	1.53	0.43	14.22	15	<.001	3.56

Note: Two-sided, one-sample Student's t test. The effect size is given by Cohen's d.

Abbreviations: ERP, event-related potential; M, mean, SD, standard deviation.

processing. Subjects' MRCP topographies before and after artifact attenuation were not significantly correlated (see Table 3), suggesting that the eye-blink dominance on the maps was removed by the artifact attenuation. Source estimation of MRCPs revealed that activity was located in central motor and parietal areas of the contralateral hemisphere (see Figure 12b). SNR of both MRCPs showed great variance before as well as after artifact handling, but their mean value remained unchanged (see Table 4). Notably, the mean SNR after artifact processing was negative ($M_{left} = -0.7$, $M_{right} = -0.3$), implying that the signal estimate was smaller than the noise estimate.

The grand mean AEP at the frontocentral ROI (channel Fz, FC1, FC2, and Cz) showed an N1 peak around 150 to 170 ms after the tone elicited by the button press, followed by a P2 around 230 ms (see Figure 12a). Before and after artifact attenuation, time courses from -100 to 300 ms of the AEP were significantly correlated (see Table 2). Averaged topographies from 150 to 170 ms after the button press exposed negativity at the frontocentral ROI resembling the AEP N1 component (Hyde, 1997). In the artifact-corrected data, the negativity peaked at the ROI, whereas in the uncorrected data the peak negativity smeared out to frontopolar channels. Nonetheless, subjects' N1 topographies before and after artifact attenuation were significantly correlated (see Table 3), suggesting that the AEP N1 was not completely shadowed by artifacts in the uncorrected dataset. Sources of the auditory N1 were estimated to be at the posterior part of the lateral fissure, nearby Heschl's gyri, the likely source of the AEP N1 (e.g., Debener, Hine, Bleeck, & Eyles, 2007; Hine & Debener, 2007). The SNR did not change after artifact attenuation, it was greater than 8 dB in both cases and its variance remained equally high before and after artifact correction (see Table 4).

4 | DISCUSSION

Currently, there is no consensus on how to deal with gait-related artifacts in mobile EEG studies. To alleviate this problem, we propose a seven-dimensional footprint

characterizing gait-related artifacts to compare objectively and comprehensively gait EEG before and after artifact attenuation. To demonstrate the utility of the gait footprint, we applied the footprint on mobile EEG data captured during free walking outdoors. We showed that features of our footprint reflect the sensitivity of two different artifact-handling stages on gait-related artifacts. To further evaluate the specificity of gait artifact handling, we measured how signals of interest remain after artifact processing (specificity).

4.1 | Sensitivity analysis: Gait-artifact–related footprint

We adapted and developed seven features capturing gait-related artifacts in multiple dimensions, such as time, time–frequency, space, and brain source space. The proposed footprint changed with different artifact attenuation stages, thereby demonstrating its sensitivity. All but two features decreased following artifact attenuation, but only two features (C and E) further decreased when ICA was performed after ASR. This shows that the footprint can be used to compare artifact attenuation pipelines more thoroughly than what is possible when only one or two features are used. We adapted features to a similar scale, to facilitate a global, cross-feature comparison. Our results indicate that the employed artifact attenuation strategy successfully reduced gait-related artifacts, albeit not equally well in every investigated dimension. Interestingly, our results suggest that the applied artifact-processing pipeline may also have reduced some of the neural activity of interest captured with EEG. The lack of a further decrease when performing ICA after ASR hints at the fact that the chosen ASR threshold ($SD = 7$) was very strict. The threshold was chosen following a previous study (Nordin et al., 2020), but is lower than the current recommendations for performing ASR to improve ICA decomposition ($SD = 20$ to $SD = 30$, Chang, Hsu, Pion-Tonachini, & Jung, 2018). Indeed, the footprint could also be used to identify suitable parameter values within a particular processing pipeline.

Some footprint features were significantly correlated before but not after artifact attenuation, indicating that properties of the EEG data changed due to artifact attenuation. Most of the moderate correlations are positive suggesting that they capture the same, multifaceted construct, i.e., gait-related artifactual activity. Feature F is adapted from a previous report investigating the walking/sitting ratio (Oliveira et al., 2016b). Before artifact attenuation, all moderate correlations of feature F with other footprint features were positive but remained insignificant (B, E). This supports the view that similar, yet non-redundant information was captured by the footprint features, indeed.
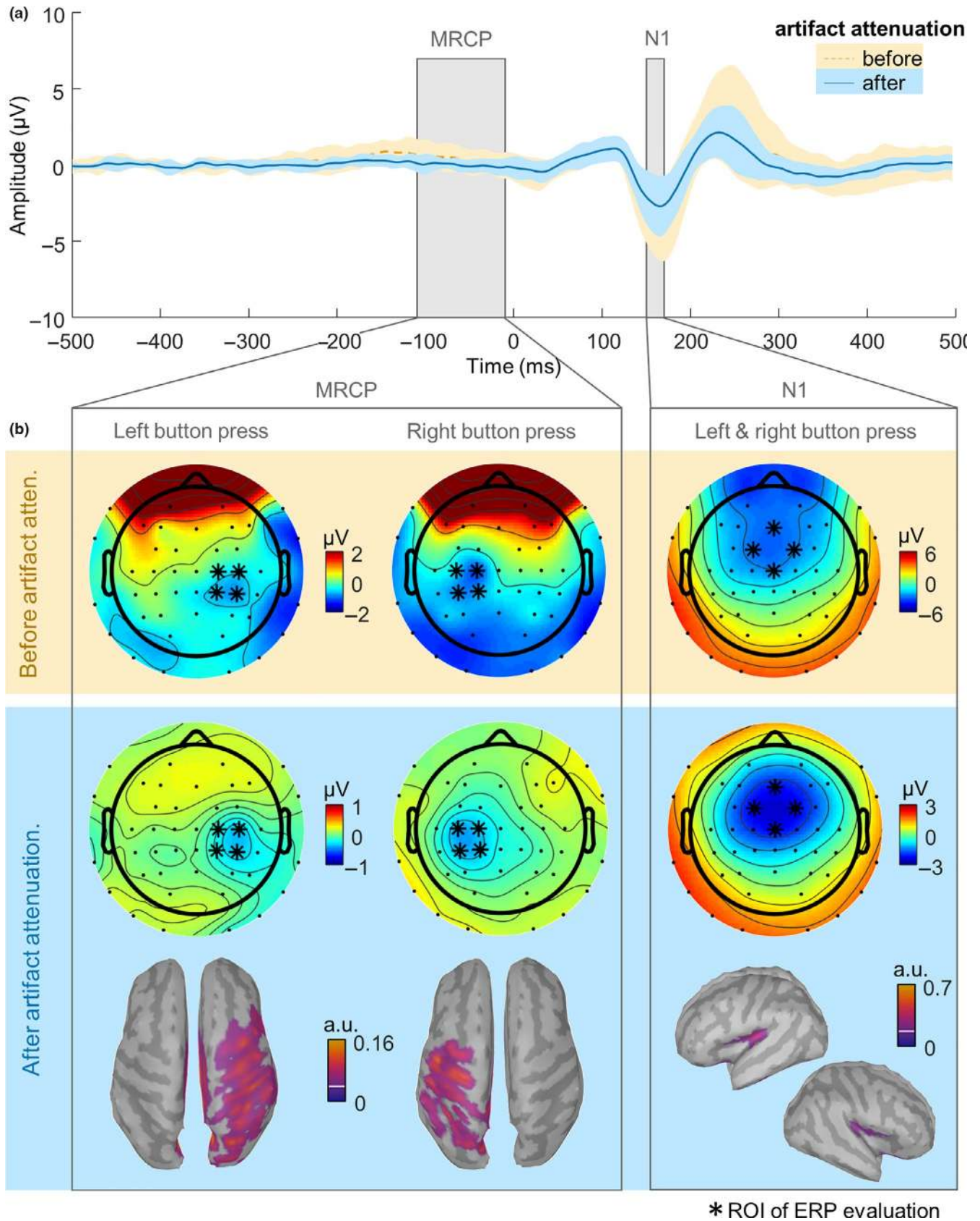
FIGURE 12 (a) Grand mean event-related potential (ERP) of the N1 region of interest (ROI). Time windows of movement-related cortical potential (MRCP) and N1 are marked by grey shaded areas. (b) Topographies of MRCPs and N1 were averaged over intervals indicated in gray in A, before (top row) and after (below) artifact processing. The bottom row illustrates source estimates of the artifact-attenuated group mean response

TABLE 3 Fisher *Z* transformed correlations of the peak topographies before and after artifact attenuation

ERP	*M*	*SD*	*T*	*df*	p_{adj}	*d*
N1	1.05	0.52	8.07	15	<0.001	2.02
MRCP left	0.11	0.33	1.28	15	1.000	0.32
MRCP right	0.00	0.44	−0.04	15	1.000	−0.01

Note: Two-sided, one-sample Student's *t* test. The effect size is given by Cohen's *d*. Abbreviations: ERP, event-related potential; *M* = mean, *SD* = standard deviation.

4.1.1 | A. EEG activity explained by head acceleration

Head acceleration magnitude explained EEG activity before but not after artifact attenuation. Previous studies of treadmill walking observed that especially vertical head acceleration shares frequency characteristics with single-channel EEG raw data, evident at higher speeds (Castermans et al., 2014; Kline et al., 2015; Nathan & Contreras-Vidal, 2016). Moreover, information from 3D head acceleration has been used to reduce motion artifacts from EEG data using adaptive filtering (Kilicarslan & Contreras Vidal, 2019). We suppose that including spatial information by using compounds of 3D head acceleration and multi-channel EEG amplitudes may provide more information, resulting in greater explained variance before artifact attenuation. Using this combined information approach should help to assess the influence of head acceleration on EEG activity better. As this feature can only be computed when head acceleration data are available, it should be investigated whether other measures of head motion (trajectory, angular velocity) yield similar results.

4.1.2 | B. Explained variance across frequencies

Power time courses of any frequency were largely predicted by time courses of all other frequencies in our walking data. After artifact attenuation, power time courses were still very similar across frequencies, hence, the decrease in this value remained insignificant. This may indicate either that some

transient artifact influence remained after artifact processing or that the proposed feature is not particularly sensitive to artifact removal. This measure also displayed little variance across subjects. We did evaluate this feature only in walking data because we were particularly interested in the motion artifact influence. It may be interesting though to evaluate whether high correlations of frequency bands are also present in standing data. Comparing explained variance across frequencies of EEG data captured during standing to EEG data captured during walking could provide a reference for future mobile EEG analysis.

4.1.3 | C. Lateral to all channel power ratio

Compared to a standing baseline, we observed a greater broadband power increase at lateral than central channels. This value decreased significantly after artifact handling. However, the size of the effect was only moderate ($d = -0.5$). This may be linked to the artifactual activity captured by lateral EEG channels (e.g., due to EMG contamination and/or electrode movement) being to a lesser extent captured by other channels, as due to the effect of volume conduction, channel recordings of EEG data are highly correlated (Buzsáki, Anastassiou, & Koch, 2012; Luck, 2014; Makeig et al., 2004). Hence, the same artifacts may influence contrasted channels resulting in greater values of this feature. Still, it seems evident that gait-related artifacts do not show evenly across the scalp (e.g., Castermans et al., 2014; Kline et al., 2015; Oliveira et al., 2016a), but which areas were most affected has not been described consistently. We found the greatest power increases to a standing baseline at lateral electrodes (see Figure 7). In line with our results, Kline et al. (2015) reported the greatest gait-related artifacts at a frontal electrode (this electrode would have been labeled as lateral in our case). Contrary to our results, Oliveira et al. (2016a) observed the greatest artifact influence at channels close to the vertex using a moving phantom head. However, they investigated artifacts of cable and electrode movement and not artifacts caused by EMG contamination, which we assume drives the increased broadband power that we observed at lateral channels.

TABLE 4 SNR of different button press ERPs before and after artifact attenuation

	Before		After					
ERP	*M*	*SD*	*M*	*SD*	*T*	*df*	*p*	*d*
MRCP left	2.12	3.80	−0.7	4.60	1.73	15	0.936	0.43
MRCP right	1.92	3.43	−0.3	3.59	1.68	15	0.936	0.42
N1	8.03	3.67	8.43	3.21	−0.8	15	1.000	−0.20

Note: Dependent samples, two-sided, Student's *t* test. The effect size is given by Cohen's *d*.
Abbreviations: ERP, event-related potential; *M* = mean, *SD* = standard deviation; SNR, signal-to-noise ratio.

4.1.4 | D. Neck channel power ratio

Before as well as after artifact attenuation, it was evident that during the double support phases electrodes placed on the side of the neck contralateral to the previous heel strike captured more broadband power than electrodes placed ipsilaterally. This is in line with a previous report (Severens et al., 2012). Keeping in mind the inconsistent results of preceding studies examining EMG activity as captures by EEG it may be interesting to examine this feature in other datasets as well. We assume that this laterality is steered by systematic gait-phase–dependent neck EMG laterality, and, thus, a ratio close to zero would be desirable. Indeed, this ratio decreased after artifact attenuation, but it did not reach zero. Still, the observed decrease indicates the effect of artifact attenuation.

4.1.5 | E. Double support power ratio

Before artifact reduction, the largest broadband power increase compared to a standing baseline occurred during double support phases. After artifact handling, we observed a small, but significant, decrease in this ratio, suggesting successful artifact reduction. Previous studies have observed broadband power increases at regions associated with motor control (SMA, premotor cortex, sensory cortex, posterior parietal cortex) mainly during double support and contralateral toe-off (e.g., Nordin et al., 2019; Oliveira, Schlink, Hairston, König, & Ferris, 2017). Hence, we did expect greater power during double than single support phases also after successful artifact handling. We suppose that the share of broadband power during double support is slightly higher than its duration in the gait cycle (here, i.e., 32%), after successful artifact handling. The double support ratio decreased after artifact attenuation to $M = 0.37$, which is close to a value that could be predicted.

4.1.6 | F. Standing/walking power ratio

Before artifact attenuation, broadband power across all channels was higher during walking than during standing. After artifact attenuation, this standing/walking power ratio decreased to values close to zero, indicating that average power during standing and walking was similar. Ratio values ranged from −0.35 to 0.59 before and from −0.56 to 0.24 after artifact processing. This result, and the fact that one subject already had a negative standing/walking ratio before artifact attenuation, illustrates the previously reported observation of fundamental inter-individual differences in gait-related artifacts (Kline et al., 2015). Our feature can be transformed into the previously described Walking/Sitting ratio if instead of EEG power of a standing baseline power of a sitting baseline

is used (Oliveira et al., 2016b). Numerically, our values were comparable to previously reported values of overground walking before and after artifact attenuation using AMICA (Arad et al., 2018). Interestingly, we did not find a strong alpha/mu or beta power decrease relative to a standing baseline after artifact attenuation over M1 (i.e., at electrode Cz, see supplemental material, Figure S4). Such power decreases have been previously reported in overground (Storzer et al., 2016) as well as exoskeleton-assisted treadmill walking (Seeber et al., 2014, 2015). In another study of unassisted treadmill walking, an alpha/mu and beta-band power decrease were only reported for one of two epilepsy patients using electrocorticography of M1 (McCrimmon et al., 2018). Hence, we argue that despite supporting evidence of the consistency of mu/alpha and beta power decreases during walking compared to standing is not known yet. Additional studies describing ERSPs relative to a standing baseline are required to determine the reliability of these power changes.

4.1.7 | G. ROI source activity

Per-vertex source activity of an ROI around M1 leg representation areas was compared to the remaining cortex before and after artifact attenuation. Contrary to our expectations, the estimated source activity of the leg motor ROI defined by us did not increase after artifact handling. This could be due to various reasons: firstly, the comparison to the remaining cortical activity might have been misleading because it included areas in which EEG source estimation has been shown to not be very sensitive (Makeig et al., 2004) or seems to be prone to artifacts (e.g., ventral and inferior medial areas). Choosing reference areas with good sensitivity for EEG source estimation that are not associated with cortical correlates of walking may be a more sensible choice in future studies. Secondly, some neural activity may have been removed by artifact handling, yielding low source activity without a clear representative spatial distribution. Thirdly, EEG source estimates benefit from digitized channel location and subject-specific neuroanatomy (e.g., magnetic resonance imaging), which were not available in the present study. As obtaining these measures requires greater resources, it would have been advantageous to show that source estimation of gait EEG is feasible without them. After all, this feature was also by far the most complex to calculate and the only one requiring an additional MATLAB toolbox (Brainstorm) besides EEGLAB.

4.2 | Specificity analyses

We performed specificity analyses to evaluate whether signals of interest remain unchanged by a particular artifact handling procedure. We observed that button-press

ERPs before and after artifact processing were correlated at central ROIs, indicating that they were similar. As the ERPs before artifact attenuation already showed a clear N1-P2 AEP following a self-elicited tone, we assume that the signal of interest was already evident before artifact attenuation and remained present afterward. Topographies of the investigated ERPs (MRCP left and right, N1) before artifact attenuation showed large influences of artifacts masking the signal, especially at frontal electrodes, probably due to blinks and eye movements. This changed after artifact attenuation. Now, ERP topographies looked as expected, that is, the MRCP showed focal negativity over contralateral central electrodes located over the primary motor cortex (e.g., Hallett, 1994) and the N1 AEP showed a peak negativity at frontocentral electrodes (e.g., Hine & Debener, 2007). As MRCP topographies changed with diminished artifacts, we expected a low correlation of the MRCP topographies before and after artifact handling (Campos Viola et al., 2009). N1 topographies before and after artifact handling were significantly correlated, demonstrating that the AEP N1 had a good signal-to-noise ratio, resulting in a robust topography. Estimated sources of the MRCP and N1 were localized close to the cortical target regions. These are areas associated with hand motor control and auditory perception, respectively. We are, therefore, confident that signals of interest remained after artifact processing. Yet, the SNR did not change after artifact attenuation. This may either indicate that the noise was not reduced or that the signal of interest was reduced in the same manner and, hence, the ratio did not change.

4.3 | Implications

The proposed footprint characterizes gait-related EEG data in various domains. A combination of all the proposed features can be merged into a single value, to describe the attenuation of gait-related artifacts. As all features can be computed individually, one may also compare single features directly. Contrary to other previously proposed features (e.g., some features of Oliveira et al., 2016b), our footprint can be calculated for single-task walking without any other ERP being present. Moreover, while some of the features may be universally applicable, other features require detailed information about gait events. Here, we share the code that is needed to calculate the footprint features, facilitating the application of the proposed footprint in future work. Given the complexity of the topic, a well-defined processing pipeline describing gait-related artifacts independent of a particular research question seems a step forward in our view.

We demonstrate that the proposed footprint could discriminate between two different artifact attenuation stages. Yet, it would be interesting to compare how well other artifact attenuation strategies perform when evaluated with the footprint. Processing pipelines may influence obtained values of footprint features allowing the optimization artifact processing by evaluating the proposed gait artifact footprint. Moreover, in the future, this footprint may be used to improve recording setups or to assess differences in gait-related artifacts between subjects (as described by, e.g., Kline et al., 2015).

In the current study, we only tested two artifact attenuation pipelines without trying to optimize any parameters. It is, therefore, possible that we did not achieve the best artifact attenuation. Still, artifact processing was reflected in a changed footprint. Besides, we do not know which part of the processed EEG data was signal and which noise. Hence, the next step would be to investigate the proposed footprint on a dataset where the ground truth is known. This could be done using simulated data or phantom head recordings with known motion parameters, neck muscle, and neural source activities (e.g., Richer et al., 2019, 2020). However, while such studies provide necessary insights, they do not replace the careful description of gait-related artifacts in natural, mobile EEG studies. Moreover, the needed equipment is only accessible to certain laboratories, as it is not commercially available, but laboratories without these possibilities may be interested in acquiring mobile gait EEG. The proposed footprint offers them a possibility to assess gait-related artifacts only using EEG data with good spatial coverage and gait event markers that could be obtained from different sensors.

5 | CONCLUSION

We conclude that the gait-related artifact footprint captures gait-related artifacts in mobile EEG data and is sensitive to artifact reduction methods. We chose artifact attenuation pipelines similar to commonly used ones, yet they may not represent the best ones available. However, the procedure serves as an example, showing that much of the gait-related artifact was suppressed in our dataset, whereas the neural activity of interest remained present.

Established features are much needed to objectively quantify the influence of gait artifacts on EEG data while walking. The proposed gait artifact footprint may serve as a valuable contribution to the growing community of mobile EEG research, as it could be used to validate different hardware choices and different artifact processing pipelines, among other applications. Further optimizing recording setups and artifact attenuation pipelines will help to establish capturing human brain function in daily life.

our gait detection procedure with a motion capture system, Reiner Emkes for hardware support, and Joanna Scanlon for her assistance during piloting. Open access funding enabled and organized by Projekt DEAL.

AUTHOR CONTRIBUTIONS

NJ collected the data and wrote the analysis scripts. SD supervised the project. All authors contributed to the design of the study and writing of the manuscript.

PEER REVIEW

The peer review history for this article is available at https://publons.com/publon/10.1111/ejn.14965.

DATA AVAILABILITY STATEMENT

MATLAB code for calculation the proposed footprint is available at GitHub (https://doi.org/10.5281/zenodo.4005945) including an example use case with data. The datasets analyzed during the current study are available in the OpenNeuro repository, https://openneuro.org/datasets/ds003039 [publicly available from August 2023].

ORCID

Nadine Svenja Josée Jacobsen 🄳 https://orcid.org/0000-0001-6612-7328

REFERENCES

Anwary, A. R., Yu, H., & Vassallo, M. (2018). Optimal foot location for placing wearable IMU sensors and automatic feature extraction for gait analysis. *IEEE Sensors Journal*, *18*(6), 2555–2567. https://doi.org/10.1109/JSEN.2017.2786587

Arad, E., Bartsch, R. P., Kantelhardt, J. W., & Plotnik, M. (2018). Performance-based approach for movement artifact removal from electroencephalographic data recorded during locomotion. *PLoS One*, *13*(5), e0197153. https://doi.org/10.1371/journal.pone.0197153

Artoni, F., Fanciullacci, C., Bertolucci, F., Panarese, A., Makeig, S., Micera, S., & Chisari, C. (2017). Unidirectional brain to muscle connectivity reveals motor cortex control of leg muscles during stereotyped walking. *NeuroImage*, *159*, 403–416. https://doi.org/10.1016/j.neuroimage.2017.07.013

Bell, A. J., & Sejnowski, T. J. (1995). An information-maximization approach to blind separation and blind deconvolution. *Neural Computation*, *7*(6), 1129–1159. https://doi.org/10.1162/neco.1995.7.6.1129

Bradford, J. C., Lukos, J. R., & Ferris, D. P. (2016). Electrocortical activity distinguishes between uphill and level walking in humans. *Journal of Neurophysiology*, *115*(2), 958–966. https://doi.org/10.1152/jn.00089.2015

Bruijn, S. M., Van Dieën, J. H., & Daffertshofer, A. (2015). Beta activity in the premotor cortex is increased during stabilized as compared to normal walking. *Frontiers in Human Neuroscience*, *9*, 593. https://doi.org/10.3389/fnhum.2015.00593

Bulea, T. C., Kim, J., Damiano, D. L., Stanley, C. J., & Park, H.-S. (2015). Prefrontal, posterior parietal and sensorimotor network activity underlying speed control during walking. *Frontiers in Human Neuroscience*, *9*, 247. https://doi.org/10.3389/fnhum.2015.00247

Buracchio, T., Dodge, H. H., Howieson, D., Wasserman, D., & Kaye, J. (2010). The trajectory of gait speed preceding mild cognitive impairment. *Archives of Neurology*, *67*(8), 980–986. https://doi.org/10.1001/archneurol.2010.159

Buzsáki, G., Anastassiou, C. A., & Koch, C. (2012). The origin of extracellular fields and currents – EEG, ECoG, LFP and spikes. *Nature Reviews Neuroscience*, *13*(6), 407–420. https://doi.org/10.1038/nrn3241

Campos Viola, F., Thorne, J., Edmonds, B., Schneider, T., Eichele, T., & Debener, S. (2009). Semi-automatic identification of independent components representing EEG artifact. *Clinical Neurophysiology*, *120*(5), 868–877. https://doi.org/10.1016/j.clinph.2009.01.015

Castermans, T., Duvinage, M., Cheron, G., & Dutoit, T. (2014). About the cortical origin of the low-delta and high-gamma rhythms observed in EEG signals during treadmill walking. *Neuroscience Letters*, *561*, 166–170. https://doi.org/10.1016/j.neulet.2013.12.059

Chang, C.-Y., Hsu, S.-H., Pion-Tonachini, L., & Jung, T.-P. (2018). Evaluation of artifact subspace reconstruction for automatic EEG artifact removal. *2018 40th Annual International Conference of the IEEE Engineering in Medicine and Biology Society (EMBC), 2018-July*(July), 1242–1245. https://doi.org/10.1109/EMBC.2018.8512547

Cromwell, R. L., Aadland-Monahan, T. K., Nelson, A. T., Stern-Sylvestre, S. M., & Seder, B. (2001). Sagittal plane analysis of head, neck, and trunk kinematics and electromyographic activity during locomotion. *Journal of Orthopaedic and Sports Physical Therapy*, *31*(5), 255–262. https://doi.org/10.2519/jospt.2001.31.5.255

Dale, A. M., Liu, A. K., Fischl, B. R., Buckner, R. L., Belliveau, J. W., Lewine, J. D., & Halgren, E. (2000). Dynamic statistical parametric mapping. *Neuron*, *26*(1), 55–67. https://doi.org/10.1016/S0896-6273(00)81138-1

De Vos, M., Gandras, K., & Debener, S. (2014). Towards a truly mobile auditory brain–computer interface: Exploring the P300 to take away. *International Journal of Psychophysiology*, *91*(1), 46–53. https://doi.org/10.1016/j.ijpsycho.2013.08.010

Debener, S., Hine, J., Bleeck, S., & Eyles, J. (2007). Source localization of auditory evoked potentials after cochlear implantation. *Psychophysiology*, *45*(1), 20–23. https://doi.org/10.1111/j.1469-8986.2007.00610.x

Debener, S., Minow, F., Emkes, R., Gandras, K., & de Vos, M. (2012). How about taking a low-cost, small, and wireless EEG for a walk? *Psychophysiology*, *49*(11), 1617–1621. https://doi.org/10.1111/j.1469-8986.2012.01471.x

Delorme, A., & Makeig, S. (2004). EEGLAB: An open source toolbox for analysis of single-trial EEG dynamics including independent component analysis. *Journal of Neuroscience Methods*, *134*(1), 9–21. https://doi.org/10.1016/j.jneumeth.2003.10.009

Delorme, A., Palmer, J., Onton, J., Oostenveld, R., & Makeig, S. (2012). Independent EEG sources are dipolar. *PLoS One*, *7*(2), e30135. https://doi.org/10.1371/journal.pone.0030135

Fisher, R. A. (1915). Frequency Distribution of the Values of the Correlation Coefficient in Samples from an Indefinitely Large Population. *Biometrika*, *10*(4), 507. https://doi.org/10.2307/2331838

Fischer, P., Chen, C. C., Chang, Y.-J., Yeh, C.-H., Pogosyan, A., Herz, D. M., … Tan, H. (2018). Alternating modulation of subthalamic nucleus beta oscillations during stepping. *Journal of Neuroscience*, *38*(22), 5111–5121. https://doi.org/10.1523/JNEUROSCI.3596-17.2018

Gramann, K., Ferris, D. P., Gwin, J., & Makeig, S. (2014). Imaging natural cognition in action. *International Journal of Psychophysiology*, *91*(1), 22–29. https://doi.org/10.1016/j.ijpsycho.2013.09.003

Gramfort, A., Papadopoulo, T., Olivi, E., & Clerc, M. (2010). OpenMEEG: Opensource software for quasistatic bioelectromagnetics. *BioMedical Engineering Online*, *9*(1), 1–20. https://doi.org/10.1186/1475-925X-9-45

Gwin, J. T., & Ferris, D. P. (2012). An EEG-based study of discrete isometric and isotonic human lower limb muscle contractions. *Journal of NeuroEngineering and Rehabilitation*, *9*(1), 35. https://doi.org/10.1186/1743-0003-9-35

Gwin, J. T., Gramann, K., Makeig, S., & Ferris, D. P. (2010). Removal of movement artifact from high-density EEG recorded during walking and running. *Journal of Neurophysiology*, *103*(6), 3526–3534. https://doi.org/10.1152/jn.00105.2010

Gwin, J. T., Gramann, K., Makeig, S., & Ferris, D. P. (2011). Electrocortical activity is coupled to gait cycle phase during treadmill walking. *NeuroImage*, *54*(2), 1289–1296. https://doi.org/10.1016/j.neuroimage.2010.08.066

Hallett, M. (1994). Movement-related cortical potentials. *Electromyography and Clinical Neurophysiology*, *34*(1), 5–13.

Hamacher, D., Herold, F., Wiegel, P., Hamacher, D., & Schega, L. (2015). Brain activity during walking: A systematic review. *Neuroscience and Biobehavioral Reviews*, *57*, 310–327. https://doi.org/10.1016/j.neubiorev.2015.08.002

Hine, J., & Debener, S. (2007). Late auditory evoked potentials asymmetry revisited. *Clinical Neurophysiology*, *118*(6), 1274–1285. https://doi.org/10.1016/j.clinph.2007.03.012

Hirasaki, E., Moore, S. T., Raphan, T., & Cohen, B. (1999). Effects of walking velocity on vertical head and body movements during locomotion. *Experimental Brain Research*, *127*(2), 117–130. https://doi.org/10.1007/s002210050781

Hyde, M. (1997). The N1 response and its applications. *Audiology and Neurotology*, *2*(5), 281–307. https://doi.org/10.1159/000259253

Kilicarslan, A., & Contreras Vidal, J. L. (2019). Characterization and real-time removal of motion artifacts from EEG signals. *Journal of Neural Engineering*, *16*(5), 056027. https://doi.org/10.1088/1741-2552/ab2b61

Kline, J. E., Huang, H. J., Snyder, K. L., & Ferris, D. P. (2015). Isolating gait-related movement artifacts in electroencephalography during human walking. *Journal of Neural Engineering*, *12*(4), 046022. https://doi.org/10.1088/1741-2560/12/4/046022

Kornhuber, H. H., & Deecke, L. (1965). Hirnpotentialänderungen bei Willkarbewegungen und passiven Bewegungen des Mensehen: Bereitschaftspotential und reafferente Potentiale. *Pfllügers Archiv Für Die Gesamte Physiologie Des Menschen Und Der Tiere*, *284*(1), 1–17.

Lau, T. M., Gwin, J. T., & Ferris, D. P. (2014). Walking reduces sensorimotor network connectivity compared to standing. *Journal of NeuroEngineering and Rehabilitation*, *11*(1), 14. https://doi.org/10.1186/1743-0003-11-14

Leutheuser, H., Gabsteiger, F., Hebenstreit, F., Reis, P., Lochmann, M., & Eskofier, B. (2013). Comparison of the AMICA and the InfoMax algorithm for the reduction of electromyogenic artifacts in EEG data. *2013 35th Annual International Conference of the IEEE Engineering in Medicine and Biology Society (EMBC)* (pp. 6804–6807). https://doi.org/10.1109/EMBC.2013.6611119

Luck, S. J. (2014). Time and frequency: A closer look at filtering and time-frequency analysis. In *An introduction to the event-related potential technique*. https://static1.squarespace.com/static/5abefa62d274cb16de90e935/t/5ac69eee575d1fe034387bd0/1522966258812/Ch_12_Time_Frequency.pdf

Luu, T. P., Brantley, J. A., Nakagome, S., Zhu, F., & Contreras-Vidal, J. L. (2017). Electrocortical correlates of human level-ground, slope, and stair walking. *PLoS One*, *12*(11), e0188500. https://doi.org/10.1371/journal.pone.0188500

Makeig, S., Debener, S., Onton, J., & Delorme, A. (2004). Mining event-related brain dynamics. *Trends in Cognitive Sciences*, *8*(5), 204–210. https://doi.org/10.1016/j.tics.2004.03.008

Makeig, S., Gramann, K., Jung, T.-P., Sejnowski, T. J., & Poizner, H. (2009). Linking brain, mind and behavior. *International Journal of Psychophysiology*, *73*(2), 95–100. https://doi.org/10.1016/j.ijpsycho.2008.11.008

McCrimmon, C. M., Wang, P. T., Heydari, P., Nguyen, A., Shaw, S. J., Gong, H., … Do, A. H. (2018). Electrocorticographic encoding of human gait in the leg primary motor cortex. *Cerebral Cortex*, *28*(8), 2752–2762. https://doi.org/10.1093/cercor/bhx155

Mullen, T. R., Kothe, C. A. E., Chi, Y. M., Ojeda, A., Kerth, T., Makeig, S., … Cauwenberghs, G. (2015). Real-time neuroimaging and cognitive monitoring using wearable dry EEG. *IEEE Transactions on Biomedical Engineering*, *62*(11), 2553–2567. https://doi.org/10.1109/TBME.2015.2481482

Nathan, K., & Contreras-Vidal, J. L. (2016). Negligible motion artifacts in scalp electroencephalography (EEG) during treadmill walking. *Frontiers in Human Neuroscience*, *9*, 708. https://doi.org/10.3389/fnhum.2015.00708

Nordin, A. D., Hairston, W. D., & Ferris, D. P. (2019). Human electrocortical dynamics while stepping over obstacles. *Scientific Reports*, *9*(1), 4693. https://doi.org/10.1038/s41598-019-41131-2

Nordin, A. D., Hairston, W. D., & Ferris, D. P. (2020). Faster gait speeds reduce alpha and beta EEG spectral power from human sensorimotor cortex. *IEEE Transactions on Biomedical Engineering*, *67*(3), 842–853. https://doi.org/10.1109/TBME.2019.2921766

O'Regan, S., Faul, S., & Marnane, W. (2013). Automatic detection of EEG artefacts arising from head movements using EEG and gyroscope signals. *Medical Engineering and Physics*, *35*(7), 867–874. https://doi.org/10.1016/j.medengphy.2012.08.017

Oliveira, A. S., Schlink, B. R., Hairston, W. D., König, P., & Ferris, D. P. (2016a). Induction and separation of motion artifacts in EEG data using a mobile phantom head device. *Journal of Neural Engineering*, *13*(3), 036014. https://doi.org/10.1088/1741-2560/13/3/036014

Oliveira, A. S., Schlink, B. R., Hairston, W. D., König, P., & Ferris, D. P. (2016b). Proposing metrics for benchmarking novel EEG technologies towards real-world measurements. *Frontiers in Human Neuroscience*, *10*, 1–15. https://doi.org/10.3389/fnhum.2016.00188

Oliveira, A. S., Schlink, B. R., Hairston, W. D., König, P., & Ferris, D. P. (2017). Restricted vision increases sensorimotor cortex involvement in human walking. *Journal of Neurophysiology*, *118*(4), 1943–1951. https://doi.org/10.1152/jn.00926.2016

Oostenveld, R., Delorme, A., & Makeig, S. (2003). DIPFIT: Equivalent dipole source localization of independent components. Retrieved from https://github.com/sccn/dipfit

Palmer, J., Kreutz-Delgado, K., & Makeig, S. (2011). AMICA: An adaptive mixture of independent component analyzers with shared

components. In Swartz Center for Computational Neuroscience, University of California, San Diego, Tech. Rep.

Pion-Tonachini, L., Kreutz-Delgado, K., & Makeig, S. (2019). The ICLabel dataset of electroencephalographic (EEG) independent component (IC) features. *Data in Brief*, *25*, 104101. https://doi.org/10.1016/j.dib.2019.104101

Pizzamiglio, S., Abdalla, H., Naeem, U., & Turner, D. L. (2018). Neural predictors of gait stability when walking freely in the real-world. *Journal of Neuroengineering and Rehabilitation*, *15*(11), 1–11. https://doi.org/10.1186/s12984-018-0357-z

Pizzamiglio, S., Naeem, U., Abdalla, H., & Turner, D. L. (2017). Neural correlates of single-and dual-task walking in the real world. *Frontiers in Human Neuroscience*, *11*(September), 1–12. https://doi.org/10.3389/fnhum.2017.00460

R Core Team (2017). *R: A language and environment for statistical computing*, Vienna, Austria: R Foundation for Statistical Computing. Retreived from https://www.r-project.org/

Reiser, J. E., Wascher, E., & Arnau, S. (2019). Recording mobile EEG in an outdoor environment reveals cognitive-motor interference dependent on movement complexity. *Scientific Reports*, *9*(1), 13086. https://doi.org/10.1038/s41598-019-49503-4

Richer, N., Downey, R. J., Hairston, W. D., Ferris, D. P., & Nordin, A. D. (2020). Motion and muscle artifact removal validation using an electrical head phantom, robotic motion platform, and dual layer mobile EEG. *IEEE Transactions on Neural Systems and Rehabilitation Engineering*, *28*(8), 1825–1835. https://doi.org/10.1109/tnsre.2020.3000971

Richer, N., Downey, R. J., Nordin, A. D., Hairston, W. D., & Ferris, D. P. (2019). Adding neck muscle activity to a head phantom device to validate mobile EEG muscle and motion artifact removal. *International IEEE/EMBS Conference on Neural Engineering, NER, 2019-March*, 275–278. https://doi.org/10.1109/NER.2019.8716959

Seeber, M., Scherer, R., Wagner, J., Solis-Escalante, T., & Müller-Putz, G. R. (2014). EEG beta suppression and low gamma modulation are different elements of human upright walking. *Frontiers in Human Neuroscience*, *8*, 485. https://doi.org/10.3389/fnhum.2014.00485

Seeber, M., Scherer, R., Wagner, J., Solis-Escalante, T., & Müller-Putz, G. R. (2015). High and low gamma EEG oscillations in central sensorimotor areas are conversely modulated during the human gait cycle. *NeuroImage*, *112*, 318–326. https://doi.org/10.1016/j.neuroimage.2015.03.045

Severens, M., Nienhuis, B., Desain, P., & Duysens, J. (2012). Feasibility of measuring event related desynchronization with electroencephalography during walking. *2012 Annual International Conference of the IEEE Engineering in Medicine and Biology Society, 2012*, 2764–2767. https://doi.org/10.1109/EMBC.2012.6346537

Sipp, A. R., Gwin, J. T., Makeig, S., & Ferris, D. P. (2013). Loss of balance during balance beam walking elicits a multifocal theta band electrocortical response. *Journal of Neurophysiology*, *110*(9), 2050–2060. https://doi.org/10.1152/jn.00744.2012

Skrandies, W. (1990). Global field power and topographic similarity. *Brain Topography*, *3*(1), 137–141. https://doi.org/10.1007/BF01128870

Snyder, K. L., Kline, J. E., Huang, H. J., & Ferris, D. P. (2015). Independent component analysis of gait-related movement artifact recorded using EEG electrodes during treadmill walking. *Frontiers in Human Neuroscience*, *9*, 639. https://doi.org/10.3389/fnhum.2015.00639

Storzer, L., Butz, M., Hirschmann, J., Abbasi, O., Gratkowski, M., Saupe, D., … Dalal, S. S. (2016). Bicycling and walking are associated with different cortical oscillatory dynamics. *Frontiers in Human Neuroscience*, *10*(February), 1–12. https://doi.org/10.3389/fnhum.2016.00061

Tadel, F., Baillet, S., Mosher, J. C., Pantazis, D., & Leahy, R. M. (2011). Brainstorm: A user-friendly application for MEG/EEG analysis. *Computational Intelligence and Neuroscience*, *2011*, 1–13. https://doi.org/10.1155/2011/879716

Venkatakrishnan, A., Francisco, G. E., Contreras-Vidal, J. (2014). Applications of brain-machine interface systems in stroke recovery and rehabilitation. *Current Physical Medicine and Rehabilitation Reports*, *2*(2), 93–105. https://doi.org/10.1007/s40141-014-0051-4

Wagner, J., Makeig, S., Gola, M., Neuper, C., & Müller-Putz, G. (2016). Distinct β band oscillatory networks subserving motor and cognitive control during gait adaptation. *Journal of Neuroscience*, *36*(7), 2212–2226. https://doi.org/10.1523/JNEUROSCI.3543-15.2016

Wagner, J., Martínez-Cancino, R., & Makeig, S. (2019). Trial-by-trial source-resolved EEG responses to gait task challenges predict subsequent step adaptation. *NeuroImage*, *199*, 691–703. https://doi.org/10.1016/j.neuroimage.2019.06.018

Wagner, J., Solis-Escalante, T., Grieshofer, P., Neuper, C., Müller-Putz, G., & Scherer, R. (2012). Level of participation in robotic-assisted treadmill walking modulates midline sensorimotor EEG rhythms in able-bodied subjects. *NeuroImage*, *63*(3), 1203–1211. https://doi.org/10.1016/j.neuroimage.2012.08.019

Wagner, J., Solis-Escalante, T., Scherer, R., Neuper, C., & Müller-Putz, G. (2014). It's how you get there: Walking down a virtual alley activates premotor and parietal areas. *Frontiers in Human Neuroscience*, *8*, 93. https://doi.org/10.3389/fnhum.2014.00093

SUPPORTING INFORMATION

Additional supporting information may be found online in the Supporting Information section.